BIOCHEMISTRY
including biophysical chemistry & molecular biology

Article

pubs.acs.org/biochemistry

Conserved Phenylalanine Residues Are Required for Blue-Shifting of Cyanobacteriochrome Photoproducts

Nathan C. Rockwell, Shelley S. Martin, Alexander G. Gulevich, and J. Clark Lagarias*

Department of Molecular and Cellular Biology, University of California, Davis, California 95616, United States

Supporting Information

ABSTRACT: Cyanobacteriochromes (CBCRs) are cyanobacterial photosensory proteins distantly related to phytochromes. Both phytochromes and CBCRs reversibly convert between dark-stable and photoproduct states upon photoisomerization of their linear tetrapyrrole (bilin) chromophores. While most phytochromes convert between a red-absorbing dark state and a far-red-absorbing photoproduct, CBCRs exhibit spectral responses spanning the entire near-ultraviolet and visible spectrum. For example, red/green CBCRs such as AnPixJ and NpR6012g4 exhibit a red-absorbing dark state similar to that of phytochrome, but photoconversion yields a green-absorbing photoproduct. "Teal-DXCF" CBCRs convert from blue- or green-absorbing dark states to yield photoproducts with very narrow absorption in the teal region of the spectrum (approximately 500 nm). The recent determination of a crystal structure of AnPixJ in its red-absorbing dark state led to the proposal that movement of a Trp residue (the "lid Trp") upon photoconversion would allow solvation of the photoproduct, thereby producing a large blue-shift. We find that substitution of the lid Trp has little effect on the NpR6012g4 photoproduct. Instead, two Phe residues conserved in red/green and teal-DXCF CBCRs are essential for determining photoproduct absorption in both CBCR groups with no significant influence on the dark-adapted state. We propose that these Phe residues constrain chromophore movement after primary photoisomerization. This work supports a trapped−twist mechanism for generating both red/green and teal-DXCF photoproducts.

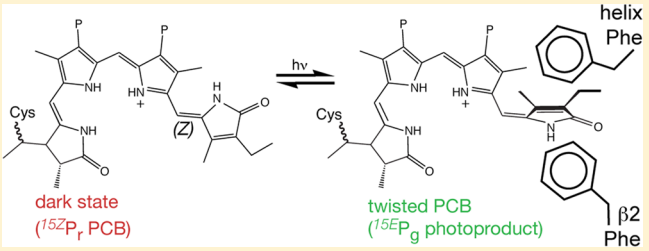

Photosensory proteins provide living cells with the ability to entrain their growth and metabolism to the ambient light environment.[2,3] Such photoreceptors have more recently been exploited to create optogenetic or synthetic photobiological research tools.[4−6] There are several superfamilies of photosensory proteins detecting light from 330 nm (near-ultraviolet)[a] to 760 nm (near-infrared) through use of a range of small organic molecules as chromophores.[b] Photoreceptors of the phytochrome superfamily are particularly interesting systems for study and engineering because they can extend further into the near-infrared range than any other known photoreceptor[2] and because of their importance in the biology of photosynthetic organisms such as crop plants.[7,8] Both phytochromes and the distantly related cyanobacteriochromes (CBCRs) incorporate linear tetrapyrroles (bilins) as chromophores, use conserved Cys residues to covalently attach the bilin to the protein, and use photoisomerization of the bilin 15,16-double bond to convert between two photostates with distinct spectral, thermal, and signaling responses.[1,9−20]

Most phytochromes convert between a dark-stable 15*Z* state and a 15*E* photoproduct.[10] The 15*Z* configuration typically absorbs red light with a peak wavelength close to that observed in samples denatured under acidic conditions, consistent with a protonated bilin chromophore.[21−23] The 15*E* photostate of phytochromes typically absorbs far-red light and thus is markedly red-shifted relative to denatured 15*E* bilins (Figure 1A).[22,23] This red-shift demonstrates the influence of the protein on the spectral properties of the chromophore: in the absence of native protein structure, the 15*E* configuration is intrinsically blue-shifted relative to the 15*Z* configuration because of steric clashes between the bilin 13- and 17-methyl groups (Figure S1 of the Supporting Information).[24] The structural basis for this spectral tuning of the phytochrome photoproduct is not yet known.[20]

CBCRs that detect far-red light have not been described. Four CBCR subfamilies have been identified to date:[2] red/green,[15,25,26] DXCF,[14,27,28] insert-Cys,[11,29] and green/red.[30,31] These subfamilies provide complete coverage of the visible and near-UV spectrum,[11,14,15,26,32,33] with known CBCR photostates including near-UV,[11] violet,[11,34] blue,[11,14,27] teal,[14,33] green,[14,25,27] yellow,[14] orange,[11,14,15,26] and red.[25,30] This diversity can seem daunting at first glance, but each CBCR subfamily employs a smaller number of allowed photostates for the 15*Z* and 15*E* configurations of the bilin chromophore. Diversity of photocycles is generated in a "mix-and-match" approach in which the allowed photostates for each bilin configuration are combined. As an example, the DXCF subfamily has known violet, blue, and green 15*Z* dark states and blue, teal, green, yellow, and orange 15*E* photoproducts.

Received: January 9, 2014
Revised: April 25, 2014
Published: April 27, 2014

   dx.doi.org/10.1021/bi500037a | *Biochemistry* 2014, 53, 3118−3130

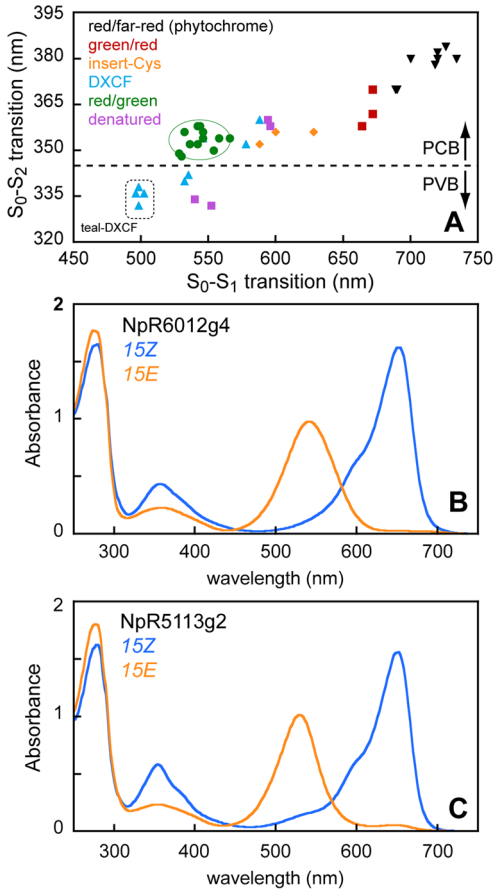

Figure 1. 15*E* photoproducts of red/green CBCRs are significantly blue-shifted. (A) Peak wavelengths for the S_0−S_1 transition (*x* axis) and S_0−S_2 transition (*y* axis, Soret band) for 15*E* photoproduct states for the indicated CBCR subfamilies relative to representative denatured samples (pink squares) and phytochromes (black triangles). Red/green CBCR photoproducts cluster in a small area, with error arcs drawn at two standard deviations for published red/green CBCRs from *Nostoc punctiforme*.[15] A Soret wavelength of 345 nm provides an approximate cutoff for CBCRs containing PCB or PVB chromophores (dashed line). The cluster of teal-DXCF proteins is indicated. (B) Spectra of the red-absorbing 15*Z* dark state (blue) and green-absorbing 15*E* photoproduct (orange) for the representative red/green CBCR NpR6012g4 from *N. punctiforme*.[15,52,62,66] (C) Spectra of the red/green CBCR NpR5113g2, which lacks the lid Trp residue of AnPixJ and NpR6012g4 (Figure S3 of the Supporting Information).[15,19]

These can be combined to yield 15 possible photocycles, eight of which have been experimentally reported.[14,27,33−36]

This mix-and-match approach means that understanding and engineering CBCR diversity revolve around understanding the tuning mechanisms that CBCRs use to generate their dark and photoproduct states. Four such tuning mechanisms have been identified. Green/red CBCRs such as RcaE and CcaS exhibit protochromic photocycles in which proton transfer between the bilin and the surrounding protein matrix produces a large change in peak absorption upon photoconversion.[30,31,37,38] DXCF and insert-Cys CBCRs use conserved "second Cys" residues to form a second thioether linkage to the chromophore at the bilin C10 atom, permitting detection of near-UV to blue light via two-Cys photocycles.[11,17,33,35,39] Some DXCF CBCRs also isomerize the chromophore precursor phycocyanobilin (PCB) into phycoviolobilin [PVB (Figure S1 of the Supporting Information)], allowing detection of teal to green light.[14,33,35,40]

In the fourth tuning mechanism, the CBCR traps a twisted photoproduct conformation in which the D-ring is effectively out of conjugation.[40] This effect was first confirmed in a subset of PVB-utilizing DXCF CBCRs that exhibit narrow teal-absorbing photoproducts (∼500 nm), the teal-DXCF proteins. In teal-DXCF proteins, the native photoproduct absorption is strikingly blue-shifted relative to that of denatured samples, an effect easily visualized by plotting peak wavelengths (Figure 1A). Like cyclic tetrapyrroles, bilins such as PCB and PVB have two absorption bands in the near-UV to visible range: a long-wavelength transition (S_0−S_1) and a second transition termed the Soret transition (S_0−S_2). In Figure 1A, the peak wavelengths for these two transitions are plotted against each other to provide a ready means of visualizing spectral tuning in the photoproduct states of experimentally characterized phytochromes and CBCRs.[11,14,15,30,31,38] The long-wavelength transitions of CBCRs containing PCB chromophores can be tuned from green to red (∼150 nm or 4100 cm^{-1}) in native samples with a much weaker effect on the Soret wavelength [∼25 nm or 1100 cm^{-1} (Figure 1A)]. Similar effects can be seen for proteins containing PVB chromophores (Figure 1A), with a blue-shift of the Soret peak relative to that of PCB due to the shorter conjugated system of PVB (Figure S1 of the Supporting Information). In teal-DXCF proteins, the peak photoproduct absorption is markedly blue-shifted relative to that of denatured PVB. Peak photoproduct absorption is not changed in these proteins upon introduction of a different bilin chromophore, in which the 18-ethyl moiety of PCB and PVB (Figure S1 of the Supporting Information) was replaced with an 18-vinyl moiety.[40] This substitution lengthens the conjugated system and hence should induce a red-shift, as was observed for both photostates of the blue/green DXCF CBCR Tlr0924 and the dark-adapted states of two teal-DXCF CBCRs.[40] However, both teal-absorbing photoproducts showed no such shift. This result implies loss of D-ring conjugation in the photoproduct but not in the dark state.

A similar blue-shift of the photoproduct relative to denatured 15*E* bilin is also seen in red/green CBCRs (Figure 1A), a subfamily including both color and power sensors that utilize PCB.[15] Red/green CBCRs such as AnPixJ and NpR6012g4 exhibit a red-absorbing 15*Z* state very similar to that of phytochrome, but the green-absorbing photoproduct is blue-shifted rather than red-shifted (Figure 1B,C). The Soret band is only slightly shifted upon photoconversion, but its intensity is notably reduced. The similarity between the red-absorbing dark states of these proteins and those of phytochromes has been borne out by the crystal structure of the red/green CBCR AnPixJ in its red-absorbing dark state.[19] In this structure, the only available structural information for any red/green CBCR to date, the PCB chromophore adopts a geometry similar to those of phytochromes in the red-absorbing dark state.[16,41−43] We previously observed a modest red-shift upon introduction of an 18-vinyl moiety into the red/green CBCRs, including NpR6012g4, and interpreted this as being inconsistent with the trapped−twist mechanism employed by teal-DXCF CBCRs for photoproduct tuning.[15] However, the recent determination of CBCR crystal structures revealed that C18 ethyl side chains of CBCRs can be substantially twisted relative to those in phytochrome structures.[17,19] To be conjugated and hence produce the observed red-shift, an 18-vinyl moiety would instead be coplanar, which complicates interpretation of this

dx.doi.org/10.1021/bi500037a | *Biochemistry* 2014, 53, 3118−3130

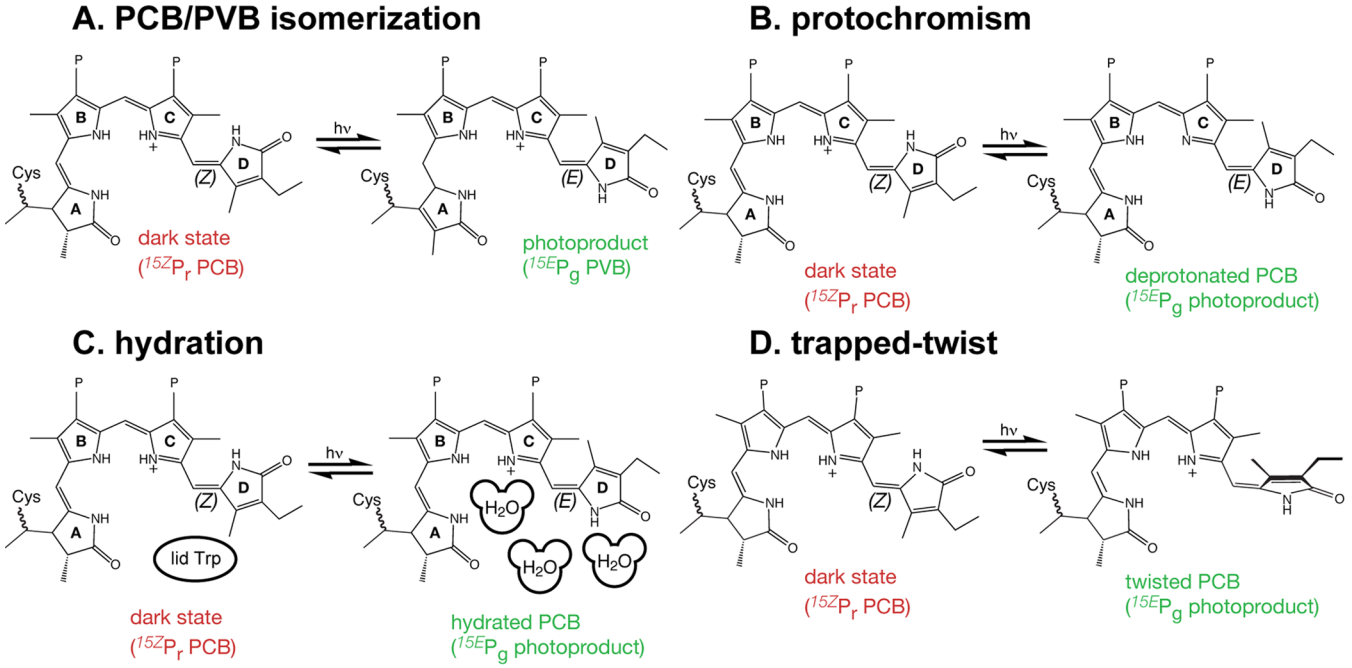

Figure 2. Proposed red/green photocycles. (A) In this model, a red-absorbing 15*Z* PCB dark state converts to a green-absorbing 15*E* PVB photoproduct via initial photoisomerization of the 15,16-double bond and subsequent ground-state isomerization of the C5 methine bridge. (B) In the protochromic model,[15] a protonated red-absorbing 15*Z* PCB dark state converts to a deprotonated green-absorbing 15*E* PCB photoproduct via photoisomerization of the 15,16-double bond and subsequent proton transfer to conserved His or Asp residues. (C) In the hydration model,[46] a desolvated red-absorbing 15*Z* PCB dark state converts to a solvated green-absorbing 15*E* PCB photoproduct via photoisomerization of the 15,16-double bond and movement of a conserved Trp residue, allowing multiple water molecules to hydrate the chromophore. (D) In the trapped−twist model,[25] a red-absorbing 15*Z* PCB dark state converts to a green-absorbing 15*E* PCB photoproduct via photoisomerization of the 15,16-double bond; after initial photoisomerization, changes in protein−chromophore interactions trap a twisted species in which the bilin D-ring cannot relax into full conjugation.

experiment. For teal-DXCF proteins containing PVB, a trapped−twist tuning mechanism is supported by structural studies of the photoactive biliprotein α-phycoerythrocyanin, in which a strongly twisted photoproduct has been observed,[44] and by spectral similarity between the teal-absorbing photoproduct and the light-harvesting pigment phycourobilin.[14,40,45] However, no equivalent information is presently available for red/green CBCR photoproducts.

Four models have been proposed to explain the properties of the green-absorbing photoproduct of red/green CBCRs such as NpR6012g4. In the first model, a red-absorbing PCB dark state leads to a green-absorbing PVB photoproduct (Figure 2A). This proposal has been only formally considered, because it is inconsistent with the native Soret wavelengths of red/green photoproducts (Figure 1A), with analysis of denatured red/green CBCRs,[15,25] and with the three intact methine bridges observed for both AnPixJ photostates using resonance Raman spectroscopy.[46] In the second model, we have argued for a protochromic photocycle with a deprotonated photoproduct, providing an explanation for the chromophore blue-shift (Figure 2B). However, the resonance Raman study of AnPixJ supports a fully protonated bilin ring system in both photostates.[46] In the third model, based on resonance Raman results and molecular dynamics simulations, a Trp residue stacked onto the AnPixJ bilin D-ring was proposed to act as a gatekeeper, maintaining a desolvated red-absorbing dark state. Photoconversion forces this "lid Trp" to move aside (Figure 2C), allowing hydration of the bilin by multiple water molecules.[46] In the fourth model,[25] the photoproduct adopts a twisted geometry with substantial deconjugation of the bilin D-ring (Figure 2D). This trapped−twist model can no longer be ruled out by the observed 18-vinyl red-shift,[15] because CBCR crystal structures reveal twisted C18 side chains. Accommodating the conjugated, coplanar 18-vinyl moiety in place of the 18-ethyl moiety could thus force a larger change in the positioning of the chromophore within the bilin-binding pocket, such that the observed red-shift could arise due to other factors.

The 15,16-photoisomerization of bilin chromophores forces a flip of the bilin D-ring relative to the C-ring (Figure S1 of the Supporting Information), so this ring must rotate in space during photoconversion. Phytochrome crystal structures typically reveal a cavity around the bilin D-ring, which presumably accommodates this rotation.[47,48] Strikingly, the dark-state AnPixJ crystal structure reveals very tight packing around the bilin D-ring compared to that in crystal structures of cyanobacterial phytochromes and of the DXCF CBCR TePixJ (Figure S2 and Tables S1 and S2 of the Supporting Information). In particular, the lid Trp residue is π-stacked onto the bilin D-ring and is apparently well positioned to restrict D-ring rotation. Were displacement of this residue to take place, hydration of the pocket might well ensue, leading to the hydration model (Figure 2C).[46] Importantly, resonance Raman spectroscopy of AnPixJ demonstrated a protonated chromophore in both photostates at pH 7.8,[46] although the pK_a of the bilin ring system in the absence of structured protein is approximately 6.[23,31] A hydrated pocket would thus seem to be at odds with the observed protonated photoproduct. Moreover, the lid Trp is not necessary for the red/green photocycle, because NpR5113g2 from *Nostoc punctiforme* exhibits a normal

dx.doi.org/10.1021/bi500037a | *Biochemistry* 2014, 53, 3118−3130

red/green photocycle (Figure 1C) but lacks the lid Trp residue (Figure S3 of the Supporting Information).[15]

In the work presented here, we revisit red/green and teal-DXCF photocycles using a series of variant proteins produced recombinantly in *Escherichia coli* engineered for coproduction of bilin chromophores.[49,50] We identify a pair of conserved Phe residues important for formation of the blue-shifted photoproducts in both CBCR groups. Available CBCR crystal structures implicate these Phe residues as providing steric constraints on evolution of the photoproduct after primary photoisomerization. Our results thus support a trapped−twist mechanism in both red/green and teal-DXCF CBCRs, identifying the trapped−twist mechanism as a powerful, widespread tool for spectral tuning of CBCR photoproducts and providing new approaches for the prediction and engineering of such behavior in other CBCRs.

MATERIALS AND METHODS

Computational Techniques. Multiple-sequence alignments of the chromophore-binding GAF domain were constructed from previous alignments[11,14,15] using manual curation based on the conserved residues highlighted in Figure S3 of the Supporting Information. For All2699g2 (second chromophore-binding domain of AphC)[26] and IflAg2 (second chromophore-binding domain of IflA),[36] spectral properties have not yet been reported for the isolated CBCR domain. We therefore aligned a region of sequence corresponding to those expressed successfully for similar domains. Superpositions of experimental crystal structures and rendering of structural figures were performed in VMD.[51]

Cloning, Mutagenesis, Expression, and Purification of CBCRs. All variant proteins were constructed by site-directed mutagenesis using the QuikChange mutagenesis system (Stratagene). Cloning, expression, and purification of NpR6012g4 have been previously described,[15,52] using well-established techniques for the coproduction of PCB in *E. coli*[49] and subsequent purification as an intein−CBD fusion.[11,52,53] Purification was performed using chitin resin (NEB) in accordance with the manufacturer's instructions; elution was performed after overnight incubation of the loaded column with dithiothreitol and final dialysis into TKKG buffer [25 mM TES-KOH (pH 7.8), 100 mM KCl, and 10% (v/v) glycerol] as described. For this study, the previously characterized regions of NpR5113g1 and NpR1597g1[14] were recloned into pET28a-RcaE[31] for expression as C-terminally His_6-tagged proteins by cloning using *Nco*I and *Bam*HI sites to keep the C-terminal His_6 tag and associated sequences in frame. Expression then used *E. coli* strain C41[DE3][54] with plasmid pKT271[50] for PCB synthesis. All purified His-tagged proteins were dialyzed into 20 mM sodium phosphate (pH 7.5), 50 mM NaCl, 10% (v/v) glycerol, and 1 mM EDTA. All constructs were verified by nucleotide sequencing. Purified protein was analyzed by sodium dodecyl sulfate−polyacrylamide gel electrophoresis using standard procedures and apparatus (Bio-Rad) followed by semidry transfer to PVDF membranes, staining with amido black for visualizing total protein, and zinc blotting[55] to confirm the presence of covalently bound bilin (Figure S4 of the Supporting Information). Some proteins were concentrated using centrifugal concentrators (10 kDa cutoff, Amicon) prior to analysis. For *in vitro* assembly assays, wild-type NpR6012g4 apoprotein and $D_{657}N$ variant NpR6012g4 in TKKG buffer were incubated at 25 °C. PCB (2 μL) was then added from a freshly prepared 1 mM stock in dimethyl sulfoxide (DMSO); this amount was determined to be saturating for P_r formation with wild-type apoprotein in pilot titration experiments.

Spectroscopic Characterization of CBCRs. Absorbance spectra were recorded at 25 °C on a Cary 50 spectrophotometer modified to permit illumination from above with a 75 W xenon source passed through a water filter and then through bandpass filters.[53] Bandpass filters [center/width (fwhm)] used for triggering photochemistry were 670 nm/40 nm, 650 nm/40 nm, 600 nm/40 nm, 580 nm/40 nm, 550 nm/70 nm, 500 nm/25 nm, and 400 nm/70 nm. CD spectra were acquired on an Applied Photophysics Chirascan instrument as described previously[11] and were used to aid the assignment of Soret peak wavelengths. Denaturation assays used a 1:6 dilution with 6 M guanidinium chloride and 100 mM citric acid (pH 2.2); photochemical characterization of denatured samples used a 320 nm long-pass filter (Schott glass WG320).[11] All photochemical difference spectra are reported as 15*Z* − 15*E*.

Gaussian Fitting of Spectra. For $F_{315}L$ NpR5113g2, photoconversion was incomplete and the two photostates were overlapped. To extract an estimated peak wavelength for the photoproduct state, we fit regions of selected CD spectra to a linear combination of normalized Gaussian functions (eq 1, where i = 2 or 3).[56]

$$A(\lambda) = \sum_i \Gamma_i(\lambda) \tag{1}$$

The individual normalized Gaussians Γ_i were of the form

$$\Gamma_i(\lambda) = I_i \times \frac{\sqrt{\frac{2}{\pi}}}{\sigma_i} \exp\left[-2\left(\frac{\lambda - \lambda_i}{\sigma_i}\right)^2\right] \tag{2}$$

where λ_i is the peak wavelength and I_i is an intensity parameter. The line width [full width at half-maximum (fwhm)] is given by eq 3.

$$\text{fwhm} = \sigma_i\sqrt{2\ln 2} \tag{3}$$

We first fit 15*Z* CD spectra from 500 to 750 nm to two Gaussian functions (eq 1 where i = 2). To fit 15*E* CD spectra, we then multiplied both fitted Gaussians from the 15*Z* spectrum by a single scaling factor (α_{12}) and used a third Gaussian to fit the 15*E* signals, yielding I_3, σ_3, and λ_3 (Table S3 of the Supporting Information). This approach implicitly assumes that photoconversion will deplete the 15*Z* spectrum with no changes in line shape. As a control, we used this procedure on NpR1597g4, a red/green CBCR known to undergo incomplete photoconversion yielding a red-shifted photoproduct, and NpR4776g2, a red/green CBCR known to undergo incomplete photoconversion yielding a normal photoproduct.[15] Derived photoproduct wavelengths for these proteins were consistent with previously assigned peak wavelengths. All derived parameters are reported in Table S3 of the Supporting Information.

RESULTS

The Red/Green Photocycle Does Not Require the Conserved Asp, His, and Trp Residues. In the AnPixJ crystal structure,[19] the chromophore is sandwiched among Trp90, Asp92, and His123. Asp92 and His123 are within conserved motifs. Phytochromes and CBCRs have a motif based on a conserved acidic residue (usually Asp); the precise composition of this motif varies among subfamilies (Figure S3 of the Supporting Information). In red/green CBCRs, this Asp

dx.doi.org/10.1021/bi500037a | *Biochemistry* 2014, 53, 3118−3130

motif is of the form Asp-Xaa-(His/Tyr)-Leu-Gln [DXXLQ (Figure S3 of the Supporting Information)]. Asp92 is the aspartate in the AnPixJ Asp motif, and His123 lies adjacent to the conserved Cys122 covalently attached to the chromophore (sometimes termed the "CH" motif, as in ref 28). Asp92 and His123 are thus candidate proton acceptor and donor residues for the protochromic model (Figure 2B). Trp90 is the lid Trp residue implicated as a critical gatekeeper in the hydration model (Figure 2C). Its side chain is stacked onto the bilin D-ring. The equivalent residues in NpR6012g4 are Asp657, His688, and Trp655. We used site-directed mutagenesis to examine the roles these residues play in the red/green photocycle of NpR6012g4. Strikingly, none of these residues are required for the red/green photocycle.

Conservative replacement of Asp657 with Asn resulted in a variant protein that failed to bind PCB upon co-expression in *E. coli* (Figure S4 of the Supporting Information). Addition of PCB to purified $D_{657}N$ NpR6012g4 apoprotein also failed to restore detectable bilin binding or photoconversion, in contrast to the case for wild-type apoprotein (Figure S5A−C of the Supporting Information). Variants in which Asp657 was replaced with Ala, Gln, or His also failed to bind bilin (Figures S4 and S5D of the Supporting Information). However, the $D_{657}E$ variant protein exhibited a red/green photocycle with a reduced level of chromophore incorporation yet only subtle changes in peak wavelength and line shape (Figure S5E of the Supporting Information and Table 1). These results demonstrate that the negative charge of Asp657 is essential for the establishment of the red-absorbing dark state, a requirement that complicates analysis of the role of this residue in photoproduct formation. We conclude that Asp657 itself is dispensable for normal photoconversion, but we cannot examine photoproduct formation in the absence of a negative charge at this position.

His688 is also dispensable. $H_{688}Q$ NpR6012g4 exhibited a normal red/green photocycle, confirming that the proton transfer ability of His is not required (Figure S6A of the Supporting Information). Other substitutions for His688 produced effects on the photoproduct state without significantly shifting the red-absorbing dark state. $H_{688}A$ and $H_{688}L$ variants exhibited similar photoproduct spectra (Figure S6B,C of the Supporting Information), with green-absorbing peaks and pronounced long-wavelength shoulders whose apparent maxima did not match those of the respective red-absorbing dark states. Denaturation analysis demonstrated that photoisomerization was not compromised in these variant proteins (Figure S6D of the Supporting Information), confirming that the long-wavelength shoulders in these variant proteins were associated with poorly photoactive 15*E* populations having peak absorption at longer wavelengths. These variants therefore formed heterogeneous photoproduct mixtures comprising a majority green-absorbing population very similar to the wild-type photoproduct and a minority population absorbing at longer wavelengths. The $H_{688}Y$ variant exhibited a red-shifted photoproduct (Figure S6E of the Supporting Information), whereas the $H_{688}C$ variant exhibited a more severe phenotype: the photoproduct was drastically red-shifted (Figure S6F of the Supporting Information and Table 1), and reverse photochemistry was no longer observed. $H_{688}E$ variant NpR6012g4 failed to bind bilin (Figures S4 and S6D of the Supporting Information). These results establish a role for His688 in tuning the NpR6012g4 photoproduct state, but it is not necessary for the red/green photocycle. Therefore, neither Asp657 nor His688 is required for the formation of the green-absorbing photoproduct of NpR6012g4, at odds with a protochromic photocycle (Figure 2B).

Table 1. Characterization of Red/Green CBCRs in This Study[a]

protein	variant	15*Z* peaks (nm)	15*E* peaks (nm)	native SAR
NpR6012g4	none (wild type)	356 (+), 650 (−)	352 (+), 542 (−)	0.98
	$A_{622}L$ (β1 notch)	356 (+), 648 (−)	360 (+), 546 (−)	1.09
	$Y_{624}H$	354, 656	358, 542	0.48
	$F_{634}V$ (β2 Phe)	356 (+), 650 (−)	358 (+), 576 (−)[c]	0.68
	$F_{634}A$	354, 652	364, 566[c]	0.28
	$A_{622}L$ $F_{634}V$	358 (+), 650 (−)	360 (+), 568 (−)[c]	0.92
	$F_{634}V$ $F_{695}L$	356, 650	364, 594[c]	0.75
	$F_{634}V$ $W_{655}H$	354, 626	356, 554	0.17
	$W_{655}H$ (lid Trp)	–	–	∼0
	$W_{655}V$	352, 642[b]	358, 542	0.66
	$W_{655}A$	352, 638[b]	358, 554	0.30
	$D_{657}N$	–	–	∼0
	$D_{657}Q$	–	–	∼0
	$D_{657}H$	–	–	∼0
	$D_{657}A$	–	–	∼0
	$D_{657}E$	356 (+), 648 (−)	356 (+), 542 (−)	0.43
	$L_{660}A$	358, 556[b]	360, 544	0.07
	$H_{688}A$	352, 638	358, 548[b]	0.31
	$H_{688}C$	354 (+), 642 (−)	360 (+), 620 (−)[c]	0.71
	$H_{688}L$	354, 640	358, 550[b]	1.25
	$H_{688}Y$	354, 640	354, 560[c]	1.18
	$H_{688}Q$	354, 638	360, 538	0.35
	$H_{688}E$	–	–	∼0
	$F_{695}L$ (helix Phe)	356 (+), 652 (−)	353 (+), 544 (−)	1.14
	$F_{695}W$	356 (+), 650 (−)	360 (+), 548 (−)	0.65
	$Y_{700}N$	354, 646	358, 539	1.19
	$Y_{718}H$	356, 648	360, 540	0.93
	$Y_{718}A$	352, 648	354, 542	0.07
NpR5113g2	none (wild type)	354 (+), 650 (−)	354 (+), 528 (−)	1.00
	$F_{256}V$ (β2 Phe)	354 (+), 650 (−)	360 (+), 584 (−)[c]	0.22
	$F_{315}L$ (helix Phe)	354 (+), 650 (−)	n/d, 570 (−)[c,d]	1.14

[a]The SAR (specific absorbance ratio) was calculated as (peak red-band absorption)/(peak 280 nm absorption). All peak wavelengths are derived from absorption spectra unless otherwise noted. Selected proteins were also characterized using CD spectroscopy; the observed CD sign is presented for such cases. [b]Significant shoulder present (see the text). [c]Value outside the observed range for wild-type red/green CBCR photoproducts (528−556 nm, NpR5113g2 and NpR6012g2, respectively).[15] [d]The peak wavelength for the 15*E* S_0−S_1 transition was estimated by fitting of CD spectra (Figure S9H and Table S4 of the Supporting Information). A similar analysis was not performed for the S_0−S_2 transition (Soret band).

We next analyzed the role of Trp655, implicated in the hydration model (Figure 2C). In AnPixJ, the $W_{90}H$ variant protein exhibits a blue-shifted dark state but a normal photoproduct.[19] This result was interpreted as arising from

dx.doi.org/10.1021/bi500037a | *Biochemistry* 2014, 53, 3118−3130

an open, hydrated pocket in the variant protein, caused by introduction of a smaller side chain. Trp90 was thus proposed to act as a critical gatekeeper or lid, desolvating the red-absorbing dark state.[46] Expression of the equivalent $W_{655}H$ variant of NpR6012g4 failed to yield stable holoprotein (Figures S4 and S7A of the Supporting Information). The lid Trp residue is not absolutely conserved in red/green CBCRs (Figure S3 of the Supporting Information). The smallest residue found at this position in characterized red/green CBCRs is Val in NpR1597g4.[15] Val is even smaller than His, so one might expect a blue-shifted NpR1597g4 dark state similar to that of the $W_{90}H$ variant of AnPixJ. This is not the case; NpR1597g4 exhibited a red-absorbing dark state with a modest blue-shift.[15] We therefore examined the $W_{655}V$ variant of NpR6012g4 (Figure S7B of the Supporting Information). In this variant, the 15*Z* dark state has a pronounced short-wavelength shoulder compared to the wild type. Subtraction of a blue-shifted wild-type spectrum from the experimental $W_{655}V$ spectrum allowed us to assign this shoulder to an apparent side population peaking at 574 nm (Figure S7C of the Supporting Information). Such a population would be spectrally similar to the 15*Z* photostate of the $W_{90}H$ variant of AnPixJ.[19] The dark state of $W_{655}A$ NpR6012g4 exhibited a more pronounced short-wavelength shoulder in the dark state relative to the $W_{655}V$ variant (Figure 3A and Table 1). The photochemical difference spectra of both variants exhibited green-absorbing 15*E* photoproducts similar to that of wild-type NpR6012g4, despite the different amounts of the proposed 15*Z* side population (Figure 3B). Subtraction of a blue-shifted, scaled 15*Z* wild-type spectrum from the absorption spectrum of 15*Z* $W_{655}A$ NpR6012g4 revealed a residual short-wavelength population similar to that observed with $W_{655}V$ NpR6012g4 (Figure 3C), with an absorption maximum at 578 nm. Characterization of the $W_{655}A$ NpR6012g4 dark state by fluorescence spectroscopy revealed a pronounced wavelength dependence in both excitation and emission spectra (Figure S7D,E of the Supporting Information). Indeed, an excitation spectrum taken at an emission wavelength of 620 nm to minimize contributions from the long-wavelength population was in good agreement with the derived absorption spectrum of the proposed side population (Figure 3C), confirming the presence of two populations.

Trp655 is close to Asp657 (Figure S3 of the Supporting Information), whose negative charge is critical for the establishment of the dark state (*vide supra*). To test whether other residues within the conserved Asp motif might also be involved in tuning the dark-state spectrum, we also characterized the $L_{660}A$ variant of NpR6012g4 (Figure 4). Leu660 in NpR6012g4 is strongly conserved in the red/green Asp motif [DXXLQ (Figure S3 of the Supporting Information)] of the red/green CBCRs. The equivalent leucine in AnPixJ, Leu95, is located below the bilin C-ring rather than the D-ring (Figure 5A). $L_{660}A$ NpR6012g4 exhibited a 15*Z* state with a majority green-absorbing population and a smaller red-absorbing side population (Figure 4A and Table 1). This phenotype is more severe than that of $W_{655}A$ NpR6012g4 (Figure 3A) but less severe than that of $W_{90}H$ AnPixJ.[19] As with other proteins in this study, we confirmed the chemical configuration of these two populations using an acid denaturation assay (Figure 4B).[22,23,57,58] Photoconversion of $L_{660}A$ NpR6012g4 also yielded a green-absorbing 15*E* photoproduct (Figure 4A,B), showing that this residue strongly

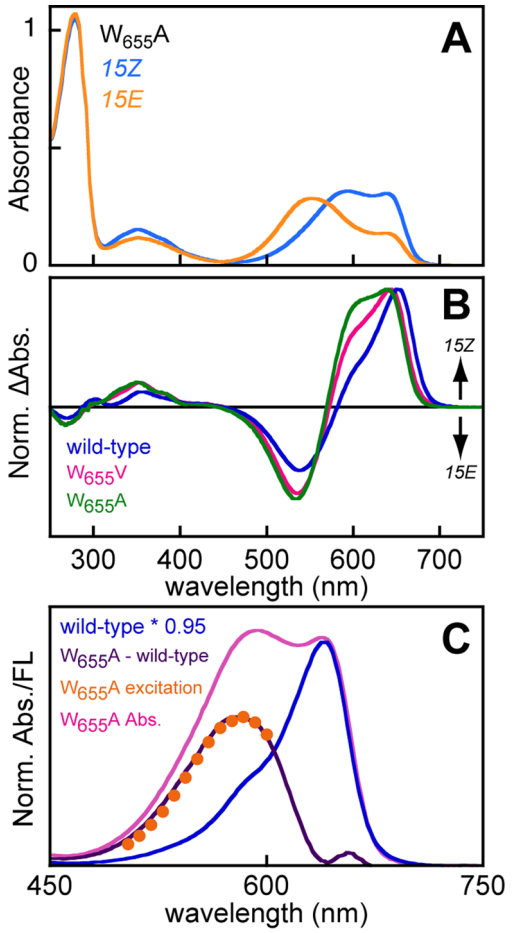

Figure 3. Trp655 is not required for the formation of the green-absorbing photoproduct in NpR6012g4. (A) Absorption spectra of $W_{655}A$ NpR6012g4 in the 15*Z* (blue) and 15*E* (orange) photostates. (B) 15*Z* − 15*E* photochemical difference spectra of wild-type (dark blue), $W_{655}V$ (magenta), and $W_{655}A$ (green) NpR6012g4. (C) The second population (deep purple) of $W_{655}A$ NpR6012g4 was resolved by subtracting the shifted wild-type spectrum scaled at 95% (dark blue) from the measured absorption spectrum (magenta). This spectrum is in good agreement with the normalized excitation spectrum recorded for $W_{655}A$ NpR6012g4 at an emission wavelength of 620 nm (orange circles).

influences the spectrum of the 15*Z* dark state without significant effects on that of the photoproduct.

Taken together, our data and the behavior of $W_{90}H$ AnPixJ demonstrate that variants replacing the lid Trp with smaller hydrophobic residues yield photoproduct states similar to those of the wild type. Such substitutions do result in the formation of a 15*Z* side population absorbing in the green to yellow region of the spectrum. These combined studies of AnPixJ and NpR6012g4 demonstrate that the severity of the phenotypes associated with the loss of the lid Trp does not correlate with the size of the residue replacing it, a result inconsistent with the hydration model. Moreover, a very similar phenotype was observed upon substitution of Leu660 in NpR6012g4, demonstrating that such phenotypes need not arise through proximity to the D-ring. We conclude that the lid Trp plays a role in the formation of the red-absorbing 15*Z* population rather than gating solvent access to the green-absorbing 15*E* chromophore.

dx.doi.org/10.1021/bi500037a | *Biochemistry* 2014, 53, 3118−3130

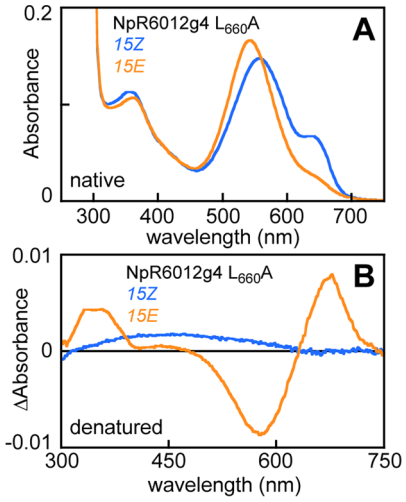

Figure 4. Leu660, like Trp655, tunes the red-absorbing dark-adapted state of NpR6012g4. (A) Absorption spectra of L_{655}A NpR6012g4 in the 15*Z* and 15*E* photostates (blue and orange curves, respectively). (B) Photochemical difference spectra of denatured L_{655}A NpR6012g4, confirming assignment of the 15*Z* and 15*E* photostates.

Photoproduct Absorption and Dark Reversion Are Modulated by Two Conserved Phe Residues. The apparent failure of both protochromic and hydration models to predict the behavior of NpR6012g4 variants underscored the need to elucidate protein residues specifically required for formation of the green-absorbing photoproduct. Interestingly, a cluster of aromatic residues is conserved in the red/green CBCR subfamily, including Phe634, Phe695, Tyr700, and Tyr718 in NpR6012g4. Phe634 is on the second strand of the central GAF β sheet. In the AnPixJ dark state, the equivalent Phe69 is immediately adjacent to the PCB C18 ethyl moiety (Figure 5B), while the corresponding residue in TePixJ (Val) is also close to the chromophore D-ring in the structure of the green-absorbing photoproduct (Figure 5C).[19] This orientation of the Phe69 side chain in AnPixJ is accommodated by a conserved small residue in the first β strand (Ala, Gly, or Ser; Ala57 in AnPixJ and Ala622 in NpR6012g4). This small residue effectively creates a "notch" for the Phe side chain (Figure 5D). The Phe634 aromatic ring of NpR6012g4 would thus be wedged between the side chains of the globally conserved Arg620 and Tyr624 residues (Figure S3 of the Supporting Information), with the latter being equivalent to Tyr176 in the red/far-red phytochrome Cph1.[59] Phe695 (Phe130 in AnPixJ) lies at the C-terminus of the helix containing His688 (Figure S3 of the Supporting Information). The equivalent Phe130 side chain is located farther from the chromophore in the AnPixJ crystal structure (Figure 5B) and interacts with the lid Trp.[19]

We reasoned that these residues might be important for tuning the photoproduct absorption because of their conservation and their proximity to the photoactive bilin D-ring. Therefore, we examined variant NpR6012g4 proteins in which these residues were replaced with equivalent residues from DXCF CBCRs (A_{622}L, F_{634}V, F_{695}L, Y_{700}N, and Y_{718}H). For the globally conserved Tyr624, which is also present in most DXCF CBCRs, we introduced a His residue, a substitution known to cause strong phenotypes in phytochrome photocycles.[59,60] These substitutions revealed that none of the three tyrosine residues was required for the red/green photocycle (Figure S8A–C of the Supporting Information and Table 1). We also examined Y_{718}A NpR6012g4, which

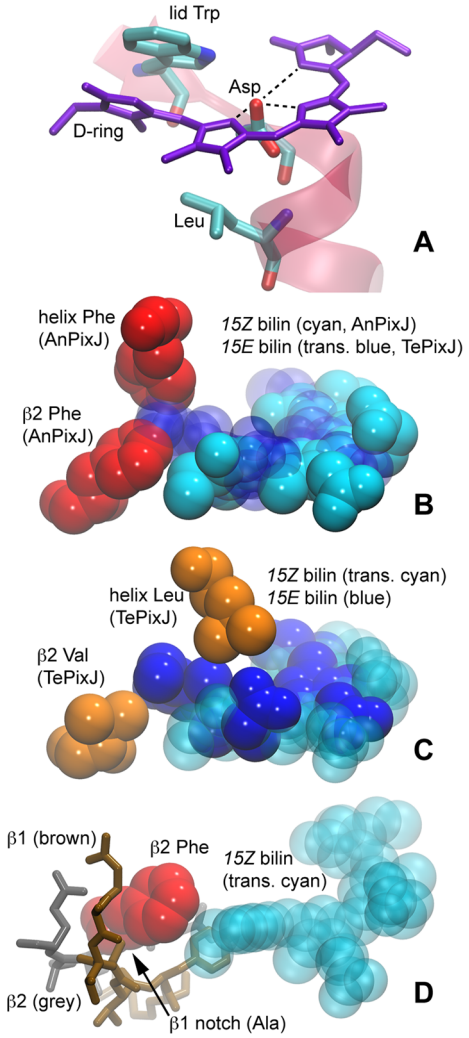

Figure 5. Protein–chromophore interactions in CBCRs AnPixJ and TePixJ. (A) In the crystal structure of AnPixJ in the 15*Z* red-absorbing photostate [Protein Data Bank (PDB) entry 3W2Z],[19] the PCB chromophore (purple) is shown with the lid Trp, Asp, and Leu residues corresponding to Trp655, Asp657, and Leu660, respectively, of NpR6012g4. The lid Trp is stacked on the D-ring; the Asp is hydrogen bonded to the NH moieties of the A-, B-, and C-rings, and the Leu is close to the C-ring on the bilin β face.[39] (B) The AnPixJ structure was superposed onto chain A of the TePixJ crystal structure in the photoproduct state (PDB entry 3VV4).[19] The β2 Phe and helix Phe residues of AnPixJ (solid red) are close to the D-ring of the 15*Z* AnPixJ chromophore (solid cyan) and exhibit steric clashes with the superposed 15*E* TePixJ chromophore (transparent blue). (C) In the same superposition shown in panel B, the TePixJ residues equivalent to the β2 Phe and helix Phe [Val and Leu, respectively (orange)] exhibit steric clashes with neither the TePixJ chromophore (solid blue) nor the AnPixJ chromophore (transparent cyan). (D) The interaction between the β2 Phe (solid red) and the chromophore (transparent cyan) in AnPixJ is facilitated by a notch formed by a small residue (Ala or Gly) on β1. β1 and β2 are colored brown and gray, respectively.

should disrupt the hydrogen bond between the chromophore D-ring and the Tyr or His residue found at this position in 15*Z* phytochrome and CBCR crystal structures.[16,17,19,41−43,47,61] Y_{718}A NpR6012g4 also exhibited a red/green photocycle, albeit with a broadened red-absorbing state (Figure S8D of the Supporting Information). Similarly, replacement of the "helix Phe" Phe695 in NpR6012g4 with either Leu or Trp or of the "β1 notch" Ala622 with Leu did not significantly affect the red/

dx.doi.org/10.1021/bi500037a | *Biochemistry* 2014, 53, 3118−3130

green photocycle (Figure S9A−C of the Supporting Information).

In contrast, we found that the β2 Phe was essential for the formation of the green-absorbing photoproduct. $F_{634}V$ NpR6012g4 exhibited a red-shifted, freely reversible photoproduct with little effect on the dark state (Figure 6A,B and

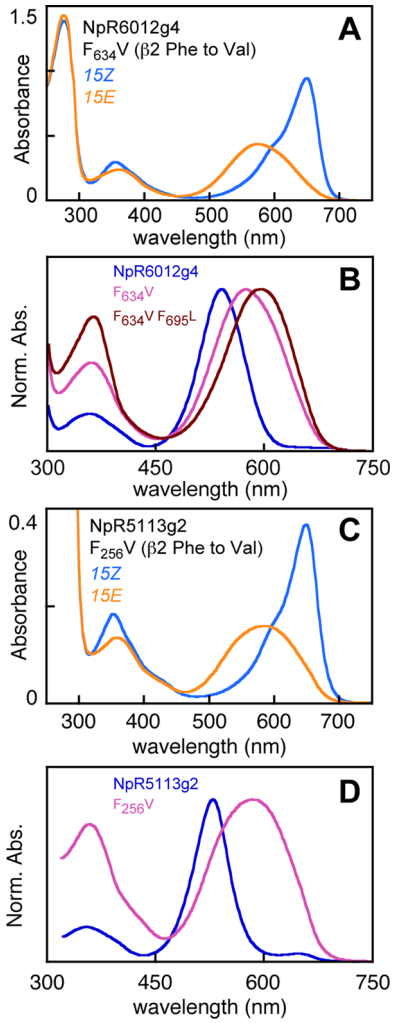

Figure 6. β2 Phe and helix Phe tune photoproduct absorption in red/green CBCRs. (A) $F_{634}V$ NpR6012g4 in the 15*Z* (blue) and 15*E* (orange) photostates. (B) Normalized absorption spectra of wild-type NpR6012g4 (dark blue), $F_{634}V$ NpR6012g4 (pink), and $F_{634}V$ $F_{695}L$ NpR6012g4 (brick red) in the photoproduct state. (C) $F_{256}V$ NpR5113g2 in the 15*Z* (blue) and 15*E* (orange) photostates. (D) Normalized absorption spectra of wild-type NpR5113g2 (dark blue) and $F_{256}V$ NpR5113g2 (pink) in the photoproduct state.

Table 1). This was not a specific effect of introducing Val at this position, because a similarly red-shifted photoproduct was also observed in the $F_{634}A$ variant (Figure S9D,E of the Supporting Information). The doubly substituted $F_{634}V$ $F_{695}L$ variant exhibited an even greater photoproduct red-shift, an effect not observed in the doubly substituted $A_{622}L$ $F_{634}V$ variant (Figure 6B and Figure S9F,G of the Supporting Information). Remarkably, the $F_{634}V$ $W_{655}H$ variant restored both chromophore binding (lost in $W_{655}H$) and the green-absorbing photoproduct (lost in $F_{634}V$), while having a broadened, blue-shifted dark state (Figure S9H of the Supporting Information Table 1). These results demonstrate that Phe634 (the β2 Phe) strongly modulates the spectral properties of the NpR6012g4 photoproduct with little effect on the red-absorbing dark state.

We next tested whether these Phe residues play a conserved role in red/green CBCRs by constructing equivalent variants of NpR5113g2, a red/green CBCR lacking the lid Trp residue (Figure S3 of the Supporting Information). In NpR5113g2, the β2 Phe is Phe256 and the helix Phe is Phe315. $F_{256}V$ NpR5113g2 exhibited a red-shifted photoproduct with little effect on the dark state (Figure 6C,D and Table 1), consistent with the behavior of $F_{634}V$ NpR6012g4. Photoconversion of $F_{315}L$ NpR5113g2 was incomplete (Figure S10A of the Supporting Information), with considerable overlap of the two photostates. However, the difference spectra of the two NpR5113g2 variants were quite similar (Figure S10B of the Supporting Information), and analysis of the CD spectra of $F_{315}L$ NpR5113g2 was consistent with partial formation of a red-shifted photoproduct (Figure S10C,D and Table S3 of the Supporting Information). Taken together, these results demonstrate that the β2 Phe is essential for the formation of the green-absorbing photoproduct in multiple red/green CBCRs, while the helix Phe can also play a role in tuning this photoproduct.

Equivalent Phe Residues Tune Teal-Absorbing Photoproducts in DXCF CBCRs. We next examined the roles that residues equivalent to Ala622, Phe634, and Phe695 might play in other CBCR subfamilies. Equivalent residues at all three positions are found in four experimentally characterized, photochemically active CBCRs: All3691, NpR1597g1, NpR5113g1, and NpR5113g3.[14,28] All four of these proteins contain only phycoviolobilin as chromophore (Figure S1 of the Supporting Information) and exhibit a narrow photoproduct absorption near 500 nm, in the teal region of the spectrum. As discussed above, such teal-absorbing photoproducts do not show a red-shift upon introduction of an 18-vinyl moiety, implicating a trapped−twist model with D-ring deconjugation.[40] We therefore chose two such proteins to explore the roles of the conserved Phe residues in "teal-DXCF" photocycles. NpR5113g1 exhibits a green-absorbing dark state and a green/teal photocycle (Figure S11A of the Supporting Information). NpR1597g1 has the blue-absorbing 15*Z* dark state typically found in DXCF CBCRs, exhibiting a blue/teal photocycle (Figure S11B of the Supporting Information) with residual blue absorption in the 15*E* photoproduct state arising because of incomplete cleavage of the second linkage.[14]

In NpR5113g1, the β2 Phe and helix Phe are Phe77 and Phe134, respectively. We examined $F_{134}L$ and $F_{77}V$ variants of NpR5113g1 (Figure 7A, Figure S12A of the Supporting Information, and Table 2). Neither substitution had a significant impact on the peak wavelength or line shape of the green-absorbing $^{15Z}P_g$ dark state (Figure 7A and Table 2). In both cases, a modest increase in absorption was observed in the blue region of the spectrum. This increase indicates that blue-absorbing, doubly linked species largely absent in wild-type NpR5113g1 (Figure S11 of the Supporting Information) are partially stabilized by these substitutions. $F_{134}L$ NpR5113g1 exhibited a teal-absorbing photoproduct with a long-wavelength shoulder (Figure S12A of the Supporting Information). $F_{77}V$ NpR5113g1 exhibited photoproduct absorption in the green region of the spectrum with no residual teal absorption, resulting in photoproduct absorption very similar to that of the blue/green DXCF CBCR TePixJ (Figure 7A,B). These results demonstrate that the β2 Phe is critical for photoproduct tuning in NpR5113g1.

dx.doi.org/10.1021/bi500037a | *Biochemistry* 2014, 53, 3118−3130

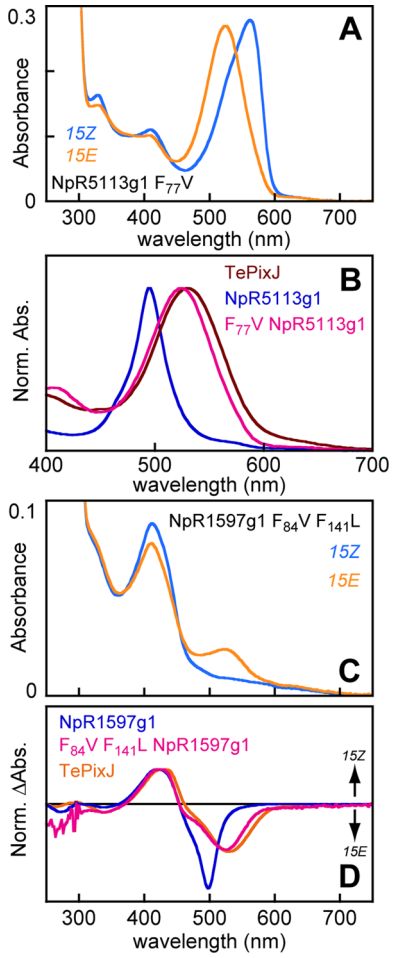

Figure 7. β2 Phe and helix Phe tune photoproduct absorption in teal-DXCF CBCRs. (A) $F_{77}V$ NpR5113g1 in the 15*Z* (blue) and 15*E* (orange) photostates. (B) Normalized absorption spectra of wild-type NpR5113g1 (dark blue), $F_{77}V$ NpR5113g1 (pink), and TePixJ (brick red) in the photoproduct state. (C) $F_{84}V$ $F_{141}L$ NpR1597g1 in the 15*Z* (blue) and 15*E* (orange) photostates. (D) Normalized photochemical difference spectra (15*Z* − 15*E*) of wild-type NpR1597g1 (dark blue), $F_{84}V$ $F_{141}L$ NpR1597g1 (pink), and TePixJ (brick red).

Table 2. Spectroscopic Parameters for Teal-DXCF CBCRs in This Study[a]

protein	variant	15*Z* peak (nm)	15*E* peak (nm)	SAR
NpR5113g1-H6	wild type	564 (564)	496 (494)	0.61
	$F_{77}V$ (β2 Phe)	400,* 562 (568)	524 (512)	0.42
	$F_{134}L$ (helix Phe)	406,* 562 (564)	408,* 498 (494)	0.07
NpR1597g1-H6	wild type	416 (420)	406,* 498 (498)	0.17
	$F_{84}V$ (β2 Phe)	416 (432)	412,* 504 (506)	0.11
	$F_{141}L$ (helix Phe)	412 (422)	408,* 498 (498)	0.09
	$F_{84}V$ $F_{141}L$	412 (424)	412,* 522 (526)	0.05

[a]The SAR was calculated as defined (Table 1). Reported peak wavelengths are from absorption spectra; values in parentheses are from photochemical difference spectra. Side populations with peak absorption at 370−450 nm are denoted with asterisks in cases in which they have been resolved.

In NpR1597g1, the β2 Phe and helix Phe are Phe84 and Phe141, respectively. $F_{141}L$ NpR1597g1 exhibited a normal doubly linked blue-absorbing dark state (Figure S12B of the Supporting Information). Photoconversion of this variant resulted in a teal photoproduct and an increase in the blue-absorbing side population relative to the wild-type population. $F_{84}V$ NpR1597g1 also had a blue-absorbing dark state similar to the wild type and retained a large blue-absorbing population after photoconversion (Figure S12C of the Supporting Information). In this variant, the teal-absorbing photoproduct exhibited a long-wavelength shoulder. We therefore characterized the $F_{84}V$ $F_{141}L$ variant of NpR1597g1, containing both substitutions. $F_{84}V$ $F_{141}L$ NpR1597g1 again exhibited a blue-absorbing dark state; photoconversion resulted in the formation of a small green-absorbing population (Figure 7D). A large blue-absorbing population was retained after photoconversion, but it was blue-shifted relative to the dark-state absorption (Table 2). The overall photochemical difference spectrum of $F_{84}V$ $F_{141}L$ NpR1597g1 was very similar to that of TePixJ (Figure 7D), with no teal-absorbing photoproduct. Thus, the $F_{84}V$ $F_{141}L$ variant protein exhibited a red-shifted photoproduct similar to those obtained by substituting the β2 Phe alone in NpR6012g4 and NpR5113g1. These results demonstrate that the β2 Phe and helix Phe play critical roles in tuning the stability and spectral properties of the photoproduct in both red/green and teal-DXCF CBCRs.

DISCUSSION

Our results provide new insight into the photocycles of red/green and teal-DXCF CBCRs and support the trapped−twist mechanism (Figure 2D) for both groups. Analysis of variant NpR6012g4 proteins revealed that the Asp and His residues implicated in a protochromic photocycle and the lid Trp residue implicated in the hydration model are all dispensable. We have identified a pair of conserved Phe residues responsible for the formation of stable blue-shifted photoproducts in multiple red/green CBCRs and in multiple teal-DXCF CBCRs. We have replaced both Phe residues in NpR6012g4 with multiple other residues, including hydrophobic residues found in other CBCRs. We cannot rule out the possibility that mutation of these residues causes structural rearrangements, and indeed, such a rearrangement is the most plausible explanation for the normal photocycle observed in the $F_{634}V$ $W_{655}H$ variant of NpR6012g4. However, the conserved role played by the β2 Phe in all four proteins tested clearly implicates this residue in photoproduct tuning. Similarly, both NpR5113g2 and NpR1597g1 also require the helix Phe for the formation of normal photoproducts.

Superposition of available CBCR crystal structures reveals a role for these residues in constraining bilin motions following photoisomerization (Figure 5B). Comparison of 15*Z* and 15*E* photostates of TePixJ (Figure S13 of the Supporting Information) provides clear evidence for the "flip-and-rotate" photoconversion mechanism also observed in bacteriophytochromes.[13,17−19,61] However, superposition of the TePixJ photoproduct on the AnPixJ dark state (Figure 5B) suggests steric clashes between the photoproduct D-ring and the β2 Phe and helix Phe that are absent with the β2 Val and helix Leu of TePixJ (Figure 5C). We therefore propose that these two Phe residues are part of a "steric blockade" that stabilizes the twisted geometry of the 15*E* photoproduct in red/green and teal-DXCF CBCRs (Figure 2D).

dx.doi.org/10.1021/bi500037a | *Biochemistry* 2014, 53, 3118−3130

Forward photoconversion of NpR6012g4 has been characterized on an ultrafast time scale,[52,62,63] while the subsequent evolution of the Lumi-R_F primary photoproduct[64] has been reported for AnPixJ.[65] Interestingly, the final intermediate observed before formation of the green-absorbing photoproduct (Figure 8) has a peak wavelength similar to those

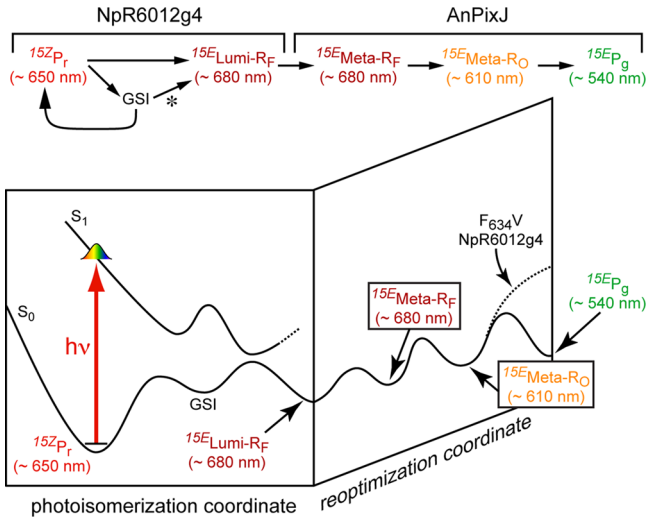

Figure 8. Proposed role of Phe residues in forward photoconversion. The top portion shows a reaction scheme for the forward photoconversion of red/green CBCRs, combining studies on NpR6012g4[52,62] and AnPixJ[25,65] and using the recently proposed nomenclature for CBCR reaction intermediates.[64] Productive formation of Lumi-R_F (asterisk) has been shown for NpR6012g4 but is not universal in red/green CBCRs.[63] The bottom portion shows a simplified, conceptual potential energy surface for the reaction scheme in the top panel. Photoisomerization generates the Lumi-R_F primary photoproduct. Subsequent evolution is shown on a "reoptimization coordinate" in which protein−chromophore interactions are reoptimized after the structural changes in Lumi-R_F formation. In the normal pathway, formation of Meta-R_F and then Meta-R_O leads to generation of the $^{15E}P_g$ photoproduct. We propose that the last step does not occur in the absence of the β2 Phe.

observed for the red-shifted photoproducts formed in variant red/green CBCRs lacking the β2 Phe residue (Figure 6 and Table 1). We therefore propose that these residues are required for this final step, in which protein−chromophore interactions are reoptimized on the ground-state electronic surface after photoisomerization (Figure 8). The precise role they play in this process is not yet clear, but we envision that they are part of a relatively rigid structure that constrains chromophore motion to trap a twisted D-ring geometry. The red-shift seen in several red/green CBCRs assembled with phytochromobilin rather than PCB[15] must indicate that this geometry retains some conjugation across the C15 methine bridge. For comparison, *in vitro* assembly of the teal-DXCF CBCR NpR5113g1 with PCB allowed characterization of a trapped−twist PCB photoproduct in an example in which no phytochromobilin red-shift occurs.[14,40] In that case, the PCB photoproduct absorbs at approximately 516 nm,[14] which is indeed more blue-shifted than the partially conjugated photoproducts of red/green CBCRs such as NpR6012g4, AnPixJ, and NpR5113g2.

Photoconversion of teal-DXCF proteins would involve generation of a similarly twisted photoproduct state, as shown both by the absence of a phytochromobilin red-shift[40] and by the conserved role of the steric blockade Phe residues in red/green CBCRs (NpR6012g4 and NpR5113g2) and teal-DXCF CBCRs (NpR5113g1 and NpR1597g1). Complete D-ring deconjugation in the teal-DXCF photoproduct also explains its spectral similarity to phycourobilin, in which both C5 and C15 are saturated, and to the α-phycoerythrocyanin photoproduct, in which C5 is saturated and the D-ring adopts a highly twisted geometry.[44,45] Interestingly, there is an also an example of a blue/teal CBCR that lacks this pair of Phe residues, Tlr1999.[33] Tlr1999 may have some type of alternative pocket, in which a different set of protein−chromophore interactions produce a similarly constrained photoproduct. Similarly, current results do not explain the red/orange photocycle reported for the CBCR domain of the tandem sensor All2699 from *Nostoc/Anabaena* sp. PCC 7120, a member of the red/green subfamily that has both blockade Phe residues but nevertheless has a red-shifted photoproduct.[26] In this case, it is possible that the absence of Gly or Pro residues in the region around the third β strand (Figure S3 of the Supporting Information) prevents the kink observed in AnPixJ[19] and results in a more spacious D-ring pocket that cannot trap the twisted photoproduct geometry. However, this hypothesis remains to be tested. An alternative pocket could also appear in the atypical CBCR NpR3784, which is distinct from red/green CBCRs at the level of primary sequence (Figure S3 of the Supporting Information) but exhibits a similar red/green photocycle.[15] Steric blockade mechanisms may also be at work in other CBCRs. For example, UV/blue and violet/orange photocycles have been reported in the insert-Cys subfamily.[11] Interestingly, the violet/orange CBCR NpF2164g3 has Val in place of the β2 Phe, while the UV/blue proteins NpF2164g2 and NpR1597g2 both have the β2 Phe (Figure S3 of the Supporting Information), potentially implicating steric blockade residues in photoproduct tuning.

Our results conflict with both protochromic and hydration models for the red/green photocycle. The potential proton acceptor residues in the NpR6012g4 pocket are not required for the red/green photocycle, inconsistent with a protochromic photocycle. The lid Trp is absent in NpR5113g2, which nevertheless has a red/green photocycle (Figure 1C). Moreover, we find no correlation between residue size and phenotype for substitutions of His688 and Trp655, arguing against a bilin-binding pocket in which the size of surrounding residues determines the photocycle by restricting or permitting hydration. Instead, we find a correlation between chemical character and phenotype: introduction of hydrophobic residues is tolerated within the red/green photocycle, albeit with formation of side populations ($W_{655}V$, $W_{655}A$, $H_{688}A$, and $H_{688}L$), but introduction of hydrogen bonding partners results in major but variable effects ($H_{688}Y$ and $H_{688}C$ in NpR6012g4 and $W_{90}H$ in AnPixJ).[19] Substitution of Ala for Leu660 also produces a phenotype very similar to that produced by substitution of the lid Trp, even though this residue is not packed onto the D-ring (Figures 4 and 5A). Amino acids 655−660 of NpR6012g4 thus seem to be critical for dark-state tuning rather than for photoproduct tuning, preventing formation of green-absorbing species that could arise through deprotonation and/or rotation about the 14,15-single bond to generate the 15-*Z*,*syn* configuration. In contrast, hydrophobic substitutions for the β2 Phe produce specific effects on photoproduct absorption even though these substitutions involve modest changes in chemical character. Conservation of key hydrophobic residues in red/green CBCRs provides further support for the steric

dx.doi.org/10.1021/bi500037a | *Biochemistry* 2014, 53, 3118−3130

blockade model: neither the helix Phe nor the lid Trp is as conserved as the β2 Phe, which is found in 95% of red/green CBCRs characterized to date (Figure S3 of the Supporting Information).

The role of the lid Trp remains enigmatic: despite its proximity to the D-ring and the phenotype of the $W_{90}H$ AnPixJ variant, this residue is not necessary for the red/green photocycle of NpR6012g4. However, replacement of the lid Trp with Val or Ala in NpR6012g4 does produce blue-shifted 15*Z* species as side populations. It is possible that NpR6012g4 differs structurally from AnPixJ, despite their homology and their similar photocycles. It is also possible that introduction of His in place of the lid Trp residue ($W_{90}H$ in AnPixJ)[19] provides a hydrogen bonding partner to stabilize a blue-shifted species that is absent or rare in wild-type proteins and is observed as a second population in $W_{655}A$ and $W_{655}V$ NpR6012g4. The dark states of both AnPixJ and NpR6012g4 are known to be heterogeneous.[46,52,62] In NpR6012g4, one subpopulation was predicted to have little or no capacity for photoconversion.[52,62] It thus becomes unclear whether the AnPixJ crystal structure[19] is that of an active or inactive configuration. Future comparative studies of red/green CBCRs using multiple experimental approaches will be required to unravel this question and to identify additional protein−chromophore interactions that provide the fascinating range of wavelength responses in CBCRs and in the phytochrome superfamily.

■ ASSOCIATED CONTENT

Supporting Information

Thirteen figures and three tables. This material is available free of charge via the Internet at http://pubs.acs.org.

■ AUTHOR INFORMATION

Corresponding Author

*Department of Molecular and Cellular Biology, 31 Briggs Hall, University of California at Davis, Davis, CA 95616. E-mail: jclagarias@ucdavis.edu. Telephone: (530) 752-1865. Fax: (530) 752-3085.

Author Contributions

N.C.R. and J.C.L. designed the study. S.S.M. and A.G.G. performed the site-directed mutagenesis, protein expression, and protein purification. N.C.R. performed all other experiments. N.C.R. and J.C.L. cowrote the manuscript.

Funding

This work was supported by a grant from the Chemical Sciences, Geosciences, and Biosciences Division, Office of Basic Energy Sciences, Office of Science, U.S. Department of Energy (DOE Grant DE-FG02-09ER16117 to J.C.L.).

Notes

The authors declare no competing financial interest.

■ ACKNOWLEDGMENTS

We thank Prof. Rei Narikawa and Prof. Masahiko Ikeuchi (University of Tokyo, Tokyo, Japan) for helpful discussions.

■ ABBREVIATIONS

Δabsorbance, change in absorbance (in difference spectra, which are reported as 15*Z* − 15*E*); CBCR, cyanobacteriochrome; CD, circular dichroism; DXCF, Asp-Xaa-Cys-Phe motif defining a subfamily of dual-Cys CBCRs; GAF, domain acronym derived from vertebrate cGMP-specific phosphodiesterases, cyanobacterial adenylate cyclases, and formate hydrogen lyase transcription activator FhlA; PCB, phycocyanobilin; PVB, phycoviolobilin; PΦB, phytochromobilin; SAR, specific absorbance ratio; TES, *N*-[tris(hydroxymethyl)methyl]-2-aminoethanesulfonic acid; X, any amino acid (e.g., in the DXCF motif).

■ ADDITIONAL NOTES

[a]Color definitions in this study are as follows: near-UV, 300−395 nm; violet, 395−410 nm; blue, 410−480 nm; teal, 480−510 nm; green, 510−570 nm; yellow, 570−585 nm; orange, 585−615 nm; red, 615−675 nm; far-red, 675−740 nm; near-IR, 740−1000 nm.

[b]Throughout, we describe photocycles using a convention whereby the 15*Z* photostate is listed first; thus, a red/green photocycle indicates that the 15*Z* photostate is red-absorbing and the 15*E* photostate is green-absorbing.[1]

■ REFERENCES

(1) Rockwell, N. C., and Lagarias, J. C. (2010) A brief history of phytochromes. *ChemPhysChem 11*, 1172−1180.

(2) Möglich, A., Yang, X., Ayers, R. A., and Moffat, K. (2010) Structure and function of plant photoreceptors. *Annu. Rev. Plant Biol. 61*, 21−47.

(3) Gomelsky, M., and Hoff, W. D. (2011) Light helps bacteria make important lifestyle decisions. *Trends Microbiol. 19*, 441−448.

(4) Möglich, A., and Moffat, K. (2010) Engineered photoreceptors as novel optogenetic tools. *Photochem. Photobiol. Sci. 9*, 1286−1300.

(5) Tabor, J. J., Levskaya, A., and Voigt, C. A. (2011) Multichromatic Control of Gene Expression in *Escherichia coli*. *J. Mol. Biol. 405*, 315−324.

(6) Müller, K., and Weber, W. (2013) Optogenetic tools for mammalian systems. *Mol. BioSyst. 9*, 596−608.

(7) Franklin, K. A., and Quail, P. H. (2010) Phytochrome functions in *Arabidopsis* development. *J. Exp. Bot. 61*, 11−24.

(8) Casal, J. J. (2013) Photoreceptor signaling networks in plant responses to shade. *Annu. Rev. Plant Biol. 64*, 403−427.

(9) Hughes, J. (2010) Phytochrome three-dimensional structures and functions. *Biochem. Soc. Trans. 38*, 710−716.

(10) Auldridge, M. E., and Forest, K. T. (2011) Bacterial phytochromes: More than meets the light. *Crit. Rev. Biochem. Mol. Biol. 46*, 67−88.

(11) Rockwell, N. C., Martin, S. S., Feoktistova, K., and Lagarias, J. C. (2011) Diverse two-cysteine photocycles in phytochromes and cyanobacteriochromes. *Proc. Natl. Acad. Sci. U.S.A. 108*, 11854−11859.

(12) Song, C., Psakis, G., Lang, C., Mailliet, J., Gartner, W., Hughes, J., and Matysik, J. (2011) Two ground state isoforms and a chromophore D-ring photoflip triggering extensive intramolecular changes in a canonical phytochrome. *Proc. Natl. Acad. Sci. U.S.A. 108*, 3842−3847.

(13) Yang, X., Ren, Z., Kuk, J., and Moffat, K. (2011) Temperature-scan cryocrystallography reveals reaction intermediates in bacteriophytochrome. *Nature 479*, 428−432.

(14) Rockwell, N. C., Martin, S. S., Gulevich, A. G., and Lagarias, J. C. (2012) Phycoviolobilin formation and spectral tuning in the DXCF cyanobacteriochrome subfamily. *Biochemistry 51*, 1449−1463.

(15) Rockwell, N. C., Martin, S. S., and Lagarias, J. C. (2012) Red/Green Cyanobacteriochromes: Sensors of Color and Power. *Biochemistry 51*, 9667−9677.

(16) Anders, K., Daminelli-Widany, G., Mroginski, M. A., von Stetten, D., and Essen, L. O. (2013) Structure of the cyanobacterial phytochrome 2 photosensor implies a tryptophan switch for phytochrome signaling. *J. Biol. Chem. 288*, 35714−35725.

(17) Burgie, E. S., Walker, J. M., Phillips, G. N., Jr., and Vierstra, R. D. (2013) A photo-labile thioether linkage to phycoviolobilin provides the foundation for the blue/green photocycles in DXCF-cyanobacteriochromes. *Structure 21*, 88−97.

(18) Cornilescu, C. C., Cornilescu, G., Burgie, E. S., Markley, J. L., Ulijasz, A. T., and Vierstra, R. D. (2014) Dynamic Structural Changes Underpin Photoconversion of a Blue/Green Cyanobacteriochrome Between its Dark and Photoactivated States. *J. Biol. Chem. 289*, 3055−3065.
(19) Narikawa, R., Ishizuka, T., Muraki, N., Shiba, T., Kurisu, G., and Ikeuchi, M. (2013) Structures of cyanobacteriochromes from phototaxis regulators AnPixJ and TePixJ reveal general and specific photoconversion mechanism. *Proc. Natl. Acad. Sci. U.S.A. 110*, 918−923.
(20) Song, C., Psakis, G., Kopycki, J., Lang, C., Matysik, J., and Hughes, J. (2014) The D-ring, Not the A-ring, Rotates in *Synechococcus* OS-B′ Phytochrome. *J. Biol. Chem. 289*, 2552−2562.
(21) Strauss, H. M., Hughes, J., and Schmieder, P. (2005) Heteronuclear solution-state NMR studies of the chromophore in cyanobacterial phytochrome Cph1. *Biochemistry 44*, 8244−8250.
(22) Ishizuka, T., Narikawa, R., Kohchi, T., Katayama, M., and Ikeuchi, M. (2007) Cyanobacteriochrome TePixJ of *Thermosynechococcus elongatus* harbors phycoviolobilin as a chromophore. *Plant Cell Physiol. 48*, 1385−1390.
(23) Shang, L., Rockwell, N. C., Martin, S. S., and Lagarias, J. C. (2010) Biliverdin amides reveal roles for propionate side chains in bilin reductase recognition and in holophytochrome assembly and photoconversion. *Biochemistry 49*, 6070−6082.
(24) Falk, H. (1989) *The Chemistry of Linear Oligopyrroles and Bile Pigments*, Springer-Verlag, Vienna.
(25) Narikawa, R., Fukushima, Y., Ishizuka, T., Itoh, S., and Ikeuchi, M. (2008) A novel photoactive GAF domain of cyanobacteriochrome AnPixJ that shows reversible green/red photoconversion. *J. Mol. Biol. 380*, 844−855.
(26) Chen, Y., Zhang, J., Luo, J., Tu, J. M., Zeng, X. L., Xie, J., Zhou, M., Zhao, J. Q., Scheer, H., and Zhao, K. H. (2012) Photophysical diversity of two novel cyanobacteriochromes with phycocyanobilin chromophores: Photochemistry and dark reversion kinetics. *FEBS J. 279*, 40−54.
(27) Yoshihara, S., Katayama, M., Geng, X., and Ikeuchi, M. (2004) Cyanobacterial Phytochrome-like PixJ1 Holoprotein Shows Novel Reversible Photoconversion Between Blue- and Green-absorbing Forms. *Plant Cell Physiol. 45*, 1729−1737.
(28) Ma, Q., Hua, H. H., Chen, Y., Liu, B. B., Kramer, A. L., Scheer, H., Zhao, K. H., and Zhou, M. (2012) A rising tide of blue-absorbing biliprotein photoreceptors: Characterization of seven such bilin-binding GAF domains in *Nostoc* sp. PCC7120. *FEBS J. 279*, 4095−4108.
(29) Lim, S., Rockwell, N. C., Martin, S. S., Lagarias, J. C., and Ames, J. B. (2013) ^{1}H, ^{15}N, and ^{13}C chemical shift assignments of cyanobacteriochrome NpF2164g3 in the photoproduct state. *Biomol. NMR Assignments*,.
(30) Hirose, Y., Shimada, T., Narikawa, R., Katayama, M., and Ikeuchi, M. (2008) Cyanobacteriochrome CcaS is the green light receptor that induces the expression of phycobilisome linker protein. *Proc. Natl. Acad. Sci. U.S.A. 105*, 9528−9533.
(31) Hirose, Y., Rockwell, N. C., Nishiyama, K., Narikawa, R., Ukaji, Y., Inomata, K., Lagarias, J. C., and Ikeuchi, M. (2013) Green/red cyanobacteriochromes regulate complementary chromatic acclimation via a protochromic photocycle. *Proc. Natl. Acad. Sci. U.S.A. 110*, 4974−4979.
(32) Ikeuchi, M., and Ishizuka, T. (2008) Cyanobacteriochromes: A new superfamily of tetrapyrrole-binding photoreceptors in cyanobacteria. *Photochem. Photobiol. Sci. 7*, 1159−1167.
(33) Enomoto, G., Hirose, Y., Narikawa, R., and Ikeuchi, M. (2012) Thiol-based photocycle of the blue and teal light-sensing cyanobacteriochrome Tlr1999. *Biochemistry 51*, 3050−3058.
(34) Song, J. Y., Cho, H. S., Cho, J. I., Jeon, J. S., Lagarias, J. C., and Park, Y. I. (2011) Near-UV cyanobacteriochrome signaling system elicits negative phototaxis in the cyanobacterium *Synechocystis* sp. PCC 6803. *Proc. Natl. Acad. Sci. U.S.A. 108*, 10780−10785.
(35) Ishizuka, T., Kamiya, A., Suzuki, H., Narikawa, R., Noguchi, T., Kohchi, T., Inomata, K., and Ikeuchi, M. (2011) The cyanobacteriochrome, TePixJ, isomerizes its own chromophore by converting phycocyanobilin to phycoviolobilin. *Biochemistry 50*, 953−961.
(36) Bussell, A. N., and Kehoe, D. M. (2013) Control of a four-color sensing photoreceptor by a two-color sensing photoreceptor reveals complex light regulation in cyanobacteria. *Proc. Natl. Acad. Sci. U.S.A. 110*, 12834−12839.
(37) Kehoe, D. M., and Grossman, A. R. (1996) Similarity of a Chromatic Adaptation Sensor to Phytochrome and Ethylene Receptors. *Science 273*, 1409−1412.
(38) Hirose, Y., Narikawa, R., Katayama, M., and Ikeuchi, M. (2010) Cyanobacteriochrome CcaS regulates phycoerythrin accumulation in *Nostoc punctiforme*, a group II chromatic adapter. *Proc. Natl. Acad. Sci. U.S.A. 107*, 8854−8859.
(39) Rockwell, N. C., Njuguna, S. L., Roberts, L., Castillo, E., Parson, V. L., Dwojak, S., Lagarias, J. C., and Spiller, S. C. (2008) A second conserved GAF domain cysteine is required for the blue/green photoreversibility of cyanobacteriochrome Tlr0924 from *Thermosynechococcus elongatus*. *Biochemistry 47*, 7304−7316.
(40) Rockwell, N. C., Martin, S. S., and Lagarias, J. C. (2012) Mechanistic Insight into the Photosensory Versatility of DXCF Cyanobacteriochromes. *Biochemistry 51*, 3576−3585.
(41) Wagner, J. R., Zhang, J., Brunzelle, J. S., Vierstra, R. D., and Forest, K. T. (2007) High resolution structure of *Deinococcus* bacteriophytochrome yields new insights into phytochrome architecture and evolution. *J. Biol. Chem. 282*, 12298−12309.
(42) Yang, X., Stojkovic, E. A., Kuk, J., and Moffat, K. (2007) Crystal structure of the chromophore binding domain of an unusual bacteriophytochrome, RpBphP3, reveals residues that modulate photoconversion. *Proc. Natl. Acad. Sci. U.S.A. 104*, 12571−12576.
(43) Essen, L. O., Mailliet, J., and Hughes, J. (2008) The structure of a complete phytochrome sensory module in the Pr ground state. *Proc. Natl. Acad. Sci. U.S.A. 105*, 14709−14714.
(44) Schmidt, M., Patel, A., Zhao, Y., and Reuter, W. (2007) Structural basis for the photochemistry of α-phycoerythrocyanin. *Biochemistry 46*, 416−423.
(45) Killilea, S. D., and O'Carra, P. (1985) Structure and apoprotein linkages of phycourobilin. *Biochem. J. 226*, 723−731.
(46) Velazquez Escobar, F., Utesch, T., Narikawa, R., Ikeuchi, M., Mroginski, M. A., Gartner, W., and Hildebrandt, P. (2013) Photoconversion Mechanism of the Second GAF Domain of Cyanobacteriochrome AnPixJ and the Cofactor Structure of Its Green-Absorbing State. *Biochemistry 52*, 4871−4880.
(47) Wagner, J. R., Brunzelle, J. S., Forest, K. T., and Vierstra, R. D. (2005) A light-sensing knot revealed by the structure of the chromophore binding domain of phytochrome. *Nature 438*, 325−331.
(48) Rockwell, N. C., and Lagarias, J. C. (2006) The structure of phytochrome. A picture is worth a thousand spectra. *Plant Cell 18*, 4−14.
(49) Gambetta, G. A., and Lagarias, J. C. (2001) Genetic engineering of phytochrome biosynthesis in bacteria. *Proc. Natl. Acad. Sci. U.S.A. 98*, 10566−10571.
(50) Mukougawa, K., Kanamoto, H., Kobayashi, T., Yokota, A., and Kohchi, T. (2006) Metabolic engineering to produce phytochromes with phytochromobilin, phycocyanobilin, or phycoerythrobilin chromophore in *Escherichia coli*. *FEBS Lett. 580*, 1333−1338.
(51) Humphrey, W., Dalke, A., and Schulten, K. (1996) VMD: Visual molecular dynamics. *J. Mol. Graphics 14*, 33−38.
(52) Kim, P. W., Freer, L. H., Rockwell, N. C., Martin, S. S., Lagarias, J. C., and Larsen, D. S. (2012) Femtosecond Photodynamics of the Red/Green Cyanobacteriochrome NpR6012g4 from *Nostoc punctiforme*. 1. Forward Dynamics. *Biochemistry 51*, 608−618.
(53) Rockwell, N. C., Shang, L., Martin, S. S., and Lagarias, J. C. (2009) Distinct classes of red/far-red photochemistry within the phytochrome superfamily. *Proc. Natl. Acad. Sci. U.S.A. 106*, 6123−6127.
(54) Miroux, B., and Walker, J. E. (1996) Over-production of proteins in *Escherichia coli*: Mutant hosts that allow synthesis of some membrane proteins and globular proteins at high levels. *J. Mol. Biol. 260*, 289−298.

(55) Berkelman, T. R., and Lagarias, J. C. (1986) Visualization of bilin-linked peptides and proteins in polyacrylamide gels. *Anal. Biochem. 156*, 194−201.
(56) Rockwell, N. C., Duanmu, D., Martin, S. S., Bachy, C., Price, D. C., Bhattacharya, D., Worden, A. Z., and Lagarias, J. C. (2014) Eukaryotic algal phytochromes span the visible spectrum. *Proc. Natl. Acad. Sci. U.S.A. 111*, 3871−3876.
(57) Zhao, K. H., Haessner, R., Cmiel, E., and Scheer, H. (1995) Type I Reversible Photochemistry of Phycoerythrocyanin Involves Z/E-Isomerization of Alpha-84 Phycoviolobilin Chromophore. *Biochim. Biophys. Acta 1228*, 235−243.
(58) Zhao, K. H., and Scheer, H. (1995) Type I and type II reversible photochemistry of phycoerythrocyanin α-subunit from *Mastigocladus laminosus* both involve Z, E isomerization of phycoviolobilin chromophore and are controlled by sulfhydryls in apoprotein. *Biochim. Biophys. Acta 1228*, 244−253.
(59) Fischer, A. J., and Lagarias, J. C. (2004) Harnessing phytochrome's glowing potential. *Proc. Natl. Acad. Sci. U.S.A. 101*, 17334−17339.
(60) Fischer, A. J., Rockwell, N. C., Jang, A. Y., Ernst, L. A., Waggoner, A. S., Duan, Y., Lei, H., and Lagarias, J. C. (2005) Multiple roles of a conserved GAF domain tyrosine residue in cyanobacterial and plant phytochromes. *Biochemistry 44*, 15203−15215.
(61) Yang, X., Kuk, J., and Moffat, K. (2008) Crystal structure of *Pseudomonas aeruginosa* bacteriophytochrome: Photoconversion and signal transduction. *Proc. Natl. Acad. Sci. U.S.A. 105*, 14715−14720.
(62) Kim, P. W., Freer, L. H., Rockwell, N. C., Martin, S. S., Lagarias, J. C., and Larsen, D. S. (2012) Second-Chance Initiation Dynamics of the Cyanobacterial Photocycle in the NpR6012 GAF4 Domain of *Nostoc punctiforme*. *J. Am. Chem. Soc. 134*, 130−133.
(63) Chang, C. W., Gottlieb, S. M., Kim, P. W., Rockwell, N. C., Lagarias, J. C., and Larsen, D. S. (2013) Reactive ground-state pathways are not ubiquitous in red/green cyanobacteriochromes. *J. Phys. Chem. B 117*, 11229−11238.
(64) Gottlieb, S. M., Kim, P. W., Corley, S. C., Madsen, D., Hanke, S. J., Chang, C. W., Rockwell, N. C., Martin, S. S., Lagarias, J. C., and Larsen, D. S. (2014) Primary and secondary photodynamics of the violet/orange dual-cysteine NpF2164g3 cyanobacteriochrome domain from *Nostoc punctiforme*. *Biochemistry 53*, 1029−1040.
(65) Fukushima, Y., Iwaki, M., Narikawa, R., Ikeuchi, M., Tomita, Y., and Itoh, S. (2011) Photoconversion mechanism of a green/red photosensory cyanobacteriochrome AnPixJ: Time-resolved optical spectroscopy and FTIR analysis of the AnPixJ-GAF2 domain. *Biochemistry 50*, 6328−6339.
(66) Kim, P. W., Freer, L. H., Rockwell, N. C., Martin, S. S., Lagarias, J. C., and Larsen, D. S. (2012) Femtosecond Photodynamics of the Red/Green Cyanobacteriochrome NpR6012g4 from *Nostoc punctiforme*. 2. Reverse Dynamics. *Biochemistry 51*, 619−630.